

## GH10 and GH11 endoxylanases in *Penicillium subrubescens*: Comparative characterization and synergy with GH51, GH54, GH62 $\alpha$ -L-arabinofuranosidases from the same fungus

Xinxin Li<sup>a</sup>, Dimitrios Kouzounis<sup>b</sup>, Mirjam A. Kabel<sup>b</sup>, Ronald P. de Vries<sup>a,\*</sup>

<sup>a</sup> Fungal Physiology, Westerdijk Fungal Biodiversity Institute & Fungal Molecular Physiology, Utrecht University, Uppsalalaan 8, 3584 CT Utrecht, The Netherlands

<sup>b</sup> Laboratory of Food Chemistry, Wageningen University & Research, Bornse Weiland 9, 6708 WG Wageningen, The Netherlands

### ARTICLE INFO

#### Keywords:

*Penicillium subrubescens*

Gene expansion

Xylan degradation

Functional diversity

Structural diversity

### ABSTRACT

*Penicillium subrubescens* has an expanded set of genes encoding putative endoxylanases (PsXLNs) compared to most other *Penicillia* and other fungi. In this study, all GH10 and GH11 PsXLNs were produced heterologously in *Pichia pastoris* and characterized. They were active towards beech wood xylan (BWX) and wheat flour arabinoxylan (WAX), and showed stability over a wide pH range. Additionally, PsXLNs released distinct oligosaccharides from WAX, and showed significant cooperative action with *P. subrubescens*  $\alpha$ -L-arabinofuranosidases (PsABFs) from GH51 or GH54 for WAX degradation, giving insight into a more diverse XLN and ABF system for the efficient degradation of complex hemicelluloses. Homology modeling analysis pointed out differences in the catalytic center of PsXLNs, which are discussed in view of the different modes of action observed. These findings facilitate understanding of structural requirements for substrate recognition to contribute to recombinant XLN engineering for biotechnological applications.

### Introduction

Xylan is the most abundant hemicellulose present in many types of lignocellulosic plant biomass, forming a complex matrix with lignin within a cellulose fibril [1]. This network is essential for the structural integrity of plants and provides resistance to pathogenic attack, pests and from enzymatic degradation [2]. Degrading xylan to overcome lignocellulose recalcitrance is essential for the efficient utilization of lignocellulose in industry. Endoxylanases (XLNs) are the most crucial enzymes for cleavage of the xylan backbone resulting in a release of xylooligosaccharides (XOS) [3]. Based on amino acid sequence similarity, fungal XLNs have been mainly classified as members of the glycoside hydrolase (GH) families GH10 and GH11 in the Carbohydrate-Active enZyme (CAZy) database (<http://www.cazy.org/>) [4]. They differ in their structure and substrate specificity [5–8].

In general, GH10 XLNs have a molecular mass of over 40 kDa and

display a salad bowl-like ( $\beta/\alpha$ )<sub>8</sub> barrel catalytic domain, with a shallow groove active site located at the larger radius on the bowl top [7,9,10]. GH11 XLNs are less than 30 kDa in size and show a hand-like  $\beta$ -jelly roll structure, with a palm active site situated between the fingers and the thumb [7,11]. In the catalytic domain, GH10 XLNs have between four and seven substrate-binding subsites, with L-arabinosyl substitutions primarily accommodated at the –3, –2 and +1 subsites and sometimes at the +2 subsite [9,10]. GH11 XLNs mostly contain five or six subsites, with the –3, +2 and +3 subsites having the ability to tolerate L-arabinosyl substitution [7,11]. The different tolerance of GH10 and GH11 XLNs to L-arabinosyl substitution explains their distinct substrate specificities and product profiles. GH10 XLNs can tolerate a higher degree of substitution on the xylan chain than GH11 XLNs, and typically result in a greater yield of shorter oligosaccharide products [6,12]. However, both GH10 and GH11 XLNs have applications in various industries, e.g. food and feed, biofuel production, pulp and paper, and medical and

**Abbreviations:** XLNs, endoxylanases; XOS, xylooligosaccharides; GH, glycoside hydrolase; CAZy, Carbohydrate-Active enZyme; ABFs,  $\alpha$ -L-arabinofuranosidases; WAX, wheat flour arabinoxylan; PsXLNs, *P. subrubescens* XLNs; PsABF, *P. subrubescens* ABFs; MEGA, Molecular Evolutionary Genetic Analysis; ML, Maximum likelihood; DNS, 3,5-dinitrosalicylic acid; BWX, beech wood xylan; HPSEC-RI, High Performance Size-Exclusion Chromatography with Refractive Index detection; HPAEC-PAD, High-Performance Anion Exchange Chromatography with Pulsed Amperometric Detection; CBM, carbohydrate-binding module; DP, degree of polymerization.

\* Corresponding author.

E-mail address: [r.devries@wi.knaw.nl](mailto:r.devries@wi.knaw.nl) (R.P. de Vries).

<https://doi.org/10.1016/j.nbt.2022.05.004>

Received 1 March 2022; Received in revised form 13 May 2022; Accepted 14 May 2022

Available online 18 May 2022

1871-6784/© 2022 The Author(s). Published by Elsevier B.V. This is an open access article under the CC BY license (<http://creativecommons.org/licenses/by/4.0/>).

pharmacological industries [13–16].

Regardless of these known differences for GH10 and GH11 XLNs, it is intriguing that some filamentous fungi possess an expanded set of XLNs of both families encoded in their genome. One of such fungi with an expanded set of XLNs is *Penicillium subrubescens* FBCC1632/CBS132785. This fungus has 10 XLN-encoding genes, a number significantly higher than that found in related fungi, e.g. *Aspergillus niger* (gene number: 5), *Trichoderma reesei* (4), *P. chrysogenum Wisconsin* (4), and *P. oxalicum* (8) [16–19]. Previously in *P. subrubescens*, it was shown that the expansion of the set of  $\alpha$ -galactosidases [20] and  $\alpha$ -L-arabinofuranosidases (ABFs) [21] resulted in functional diversity. While those studies both addressed exo-acting enzymes, in this study the aim was to reveal whether such functional diversification also occurred for the expanded set of XLNs, or whether this largely resulted in enzymatic redundancy.

For this, the genes encoding three GH10 and seven GH11 XLNs in *P. subrubescens* were heterogeneously expressed in *Pichia pastoris*. The recombinant proteins were characterized, and the product profiles towards wheat flour arabinoxylan (WAX) hydrolysis, followed by homology modeling analysis, were used to understand enzyme interactions with decorated heteroxylan. Moreover, the cooperative action of *P. subrubescens* XLNs (PsXLNs) with *P. subrubescens* ABFs (PsABF) was assessed to find leads to improve existing enzyme cocktails degrading dietary fiber rich in WAX.

## Materials and methods

### Phylogenetic analysis of fungal GH10 and GH11 XLNs

All fungal amino acid sequences in this study were obtained from JGI Mycocosm (<https://mycocosm.jgi.doe.gov/mycocosm/home>) [22] and the CAZY database (<http://www.cazy.org/>) [4] (Supplementary Table S1). Their signal peptides were predicted using SignalP v5.0 (<http://www.cbs.dtu.dk/services/SignalP/>) and removed manually [23]. Sequences without signal peptides were aligned with the MAFFT server (<https://www.ebi.ac.uk/Tools/msa/mafft/>) [24] and further analyzed in the Molecular Evolutionary Genetic Analysis software version 7 (MEGA7) [25]. Maximum likelihood (ML) was run in MEGA, using 500 bootstrap re-samplings with 95% partial deletion of gap under the Poisson correction distance of substitution rates. Three characterized plant GH10 XLNs were used as an outgroup of the GH10 tree [26–28], whereas three characterized bacterial GH11 XLNs were used as an outgroup of the GH11 tree [29–31].

### Cloning of *P. subrubescens* XLN-encoding genes and transformation to *Pichia pastoris*

Total RNA of *P. subrubescens* was extracted and purified as described previously [20]. Full-length cDNA was obtained with ThermoScript Reverse Transcriptase (Invitrogen, Carlsbad, CA, USA) using total RNA as a template. The mature XLN-encoding genes without the native signal peptide-coding sequence were amplified from full-length cDNA using the specific primers (Supplementary Table S2). The PCR products were purified and digested with the appropriate restriction enzymes (Promega, Madison, WI, USA). The digested products were ligated into pPICZ $\alpha$ A vector and transformed into *Escherichia coli* DH5 $\alpha$  competent cells for propagation and sequencing. The recombinant plasmids were subsequently extracted from strains containing DNA of the correct sequence, linearized with *PmeI* (Promega), and then transformed by electroporation using a BioRad GenePulser (BioRad, Hercules, CA, USA) into *P. pastoris* strain X-33.

### Production and purification of recombinant XLNs

The *P. pastoris* transformants with the highest production level were selected using colony Western Blot as described previously [32], and further cultured in YPD (yeast peptone dextrose medium) and BMGY

(buffered glycerol complex medium) sequentially. Induction was done in BMMY (buffered methanol complex medium) medium at 22 °C, 280 rpm with methanol being supplemented to 1% (v/v) every 24 h for 96 h. Culture supernatants were harvested (8000g, 4 °C, 20 min), concentrated by Vivaflow 200 membrane of 10 kDa molecular weight cutoff (Sartorius AG, Goettingen, Germany), and purified using an ÄKTA FPLC device (GE Life Sciences, Uppsala, Sweden) at 4 °C. Crude enzymes were loaded onto a HisTrap FF 1 mL column (Cytiva, Marlborough, MA, USA) equilibrated with 20 mM HEPES, 0.4 M NaCl, 20 mM imidazole, pH 7.5, and eluted using a linear gradient of 22–400 mM imidazole in buffer mentioned above at a flow rate of 1.0 mL/min [20]. Fractions containing enzyme were collected, concentrated and buffer-exchanged to 20 mM HEPES (pH 7.0) using 10 kDa cut-off ultrafiltration units Amicon (Merck Millipore, Bedford, MA, USA) [20]. The concentration of purified enzymes were determined using the Bradford method with bovine serum albumin (Pierce, Thermo Fisher Scientific, Loughborough, UK) as a standard (5–1000  $\mu$ g/mL). These purified enzymes were filtered through 0.22  $\mu$ m filters and stored at 4 °C prior to further analysis biochemical properties and hydrolysis patterns.

### XLN activity assays and the effects of temperature and pH

XLN activity was determined by using the DNS (3,5-dinitrosalicylic acid) method [33]. Xylan from beech wood (BWV, Carl Roth GmbH, Karlsruhe, Germany) and wheat flour (medium) (WAX, P-WAXYM, Megazyme, Wicklow, Ireland) were used as substrates. The standard reaction was performed with 20  $\mu$ L of diluted purified enzyme and 60  $\mu$ L of 0.5% (w/v) xylan in 100 mM NaOAc buffer (pH 5.0) at 40 °C, 110 rpm, for 10 min. The reaction was then stopped by adding 120  $\mu$ L DNS reagent, and incubated at 95 °C for 10 min. After cooling to room temperature, the absorbance at 540 nm was measured in a 96 well microplate. The reaction systems without enzymes were treated as the control. All experiments were carried out in triplicate. One unit (U) of XLN activity was defined as the amount of enzyme releasing 1  $\mu$ mol of xylose per min under the standard assay condition.

Temperature and pH optima of XLNs were determined at 30–90 °C in 100 mM NaOAc buffer, pH 5.0, or at 40 °C in 100 mM citric acid-Na<sub>2</sub>HPO<sub>4</sub> buffer, pH 3.0–8.0, respectively. Thermal and pH stability of XLNs were estimated by measuring the residual enzyme activities under standard condition after 1 h pre-incubation without substrate. For assay of thermal stability, the 1 h pre-incubation was performed at 30–90 °C in 100 mM NaOAc buffer (pH 5.0). For assay of pH stability, the 1 h pre-treatment was carried out at 30 °C in 100 mM citric acid-Na<sub>2</sub>HPO<sub>4</sub> buffer (pH 2.0–8.0), Tris-NaCl buffer (pH 8.0–9.0), and glycine-NaOH buffer (pH 9.0–11.0).

### Hydrolysis of WAX by each independent XLN and analysis of product profile

To investigate the product profile of WAX hydrolysis by each individual PsXLN, 5  $\mu$ g/mL XLN was incubated with 0.5% (w/v) WAX in 50 mM NaOAc buffer (pH 5.0) at 40 °C, 16 h, under continuous agitation. The reaction without the addition of enzymes was treated as control. All reactions were ended by incubating at 99 °C for 15 min, and centrifuged for 10 min (20,000g, 15 °C). The supernatants were diluted twice and 20 times prior to their HPSEC-RI (High Performance Size-Exclusion Chromatography with Refractive Index detection) and HPAEC-PAD (High-Performance Anion Exchange Chromatography with Pulsed Amperometric Detection) analysis, respectively.

### Molecular weight distribution determination by HPSEC-RI

The molecular weight distribution of XLN-treated and untreated WAX was determined by HPSEC-RI, according to [34]. Analysis was performed with an Ultimate 3000 HPLC System (Dionex Corp., Sunnyvale, CA, USA) equipped 4000AW, 3000AW, and 2500AW TSK-Gel

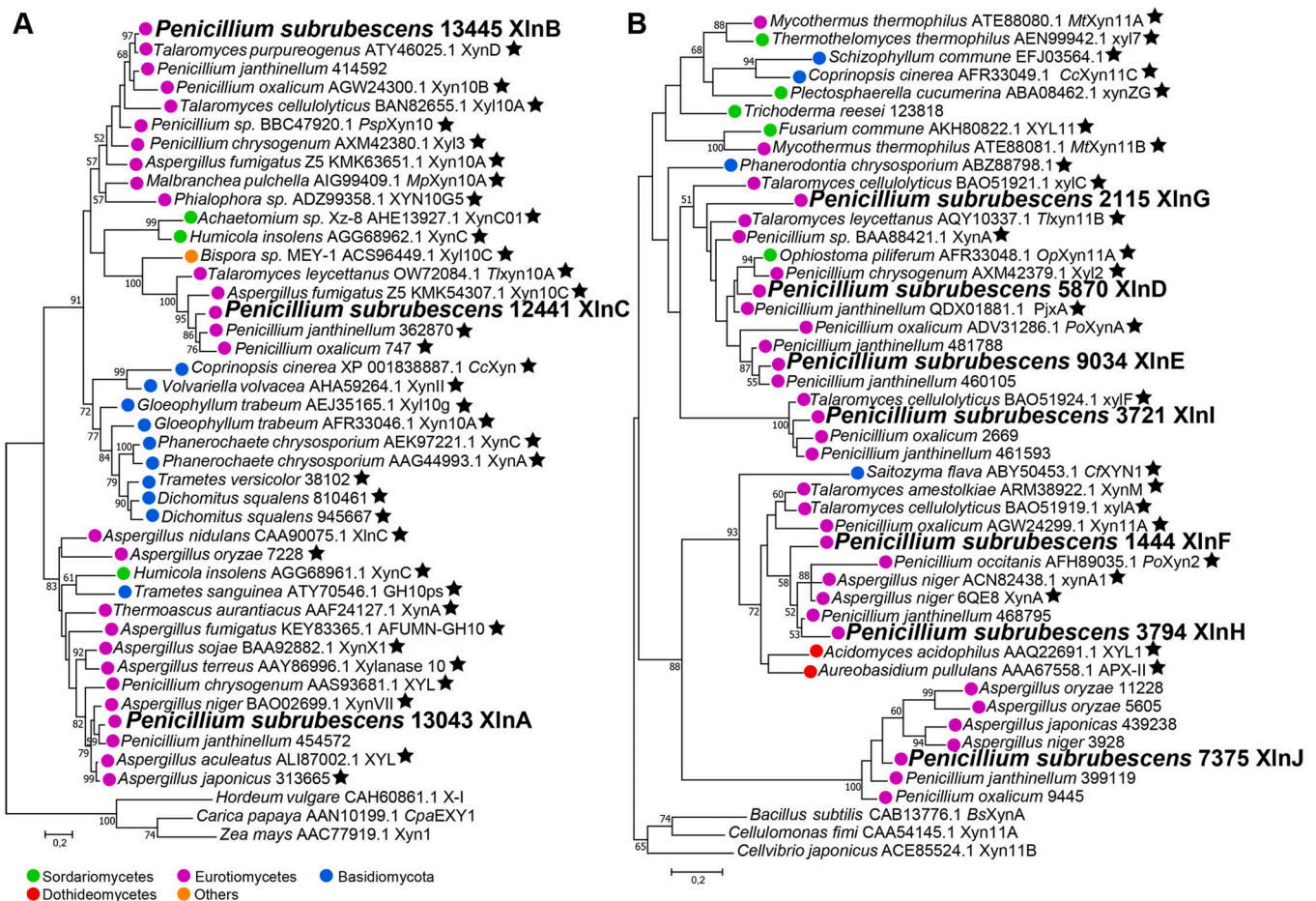


**Fig. 1.** Analysis of phylogenetic relationships among the (putative) fungal XLNs from *P. subrubescens* and selected fungal species from GH10 (A) and GH11 (B). The phylogenetic tree shown was based on the ML method. Only bootstrap values above 50% are shown next to the branches to support nodes. The putative *P. subrubescens* XLNs are highlighted in bold. The previously characterized XLNs are indicated by black stars.

Super columns (6 mm ID × 150 mm per column, 6 μm), and a TSK Super AW-L guard column (4.6 mm ID × 35 mm, 7 μm) (Tosoh Bioscience, Tokyo, Japan). The HPLC system was coupled to an ERC Refractomax 520 detector (Biotech AB, Onsala, Sweden). The system was calibrated using a pullulan series of known MW (Sigma Aldrich, St. Louis, MO, USA).

#### Product profiling by HPAEC-PAD

Mono- and oligosaccharides were profiled by HPAEC-PAD. Analysis was performed with an ICS7000 HPLC system (Dionex), coupled with an ISC7000 ED PAD detector (Dionex) and equipped with a CarboPac™ PA1 IC column (250 mm × 2 mm i.d.) and a CarboPac™ PA guard column (50 mm × 2 mm i.d.). 0.1 M sodium hydroxide (NaOH) (A) and 1 M sodium acetate in 0.1 M NaOH (B) were used as mobile phases. Analysis was performed by injecting 10 μL, at 0.3 mL/min (20 °C) using the following elution profile: 0 – 32 min from 0% to 38% B (linear gradient), 32 – 37 min from 32% to 100% B, 37 – 42 min at 100% B (isocratic), 42 – 42.1 min to 100% A (linear gradient) and 42.1 – 55 min 100% A (isocratic).

For comparison and annotation of peaks, product profiles of WAX digested by commercially available and well characterized TmGH10 (*Thermotoga maritima*, E-XYLATM) and NpGH11 (*Neocallimastix patriciarum*, E-XYLNP, [35]), as well as standards (10 – 20 μg/mL, XOS, A<sup>2</sup>XX, XA<sup>3</sup>XX, XA<sup>2</sup>XX, A<sup>2+3</sup>XX, Megazyme) are included in this study. Additional peaks were putatively annotated based on the HPAEC elution pattern of AXOS, previously reported by [36].

#### Synergy with ABF for soluble sugar production

To investigate the cooperative action between each individual PsXLN and different PsABFs, 0.6 μM of each PsXLN was simultaneously incubated with 6 μM PsABF for the hydrolysis of 0.5% (w/v) WAX in 100 mM NaOAc buffer (pH 5.0) at 40 °C, 110 rpm, 24 h. The reaction systems without enzymes or with only a single PsXLN were treated as controls. The amount of reducing sugars released was determined by the DNS method as mentioned above. All the above hydrolysis assays were carried out in triplicate.

#### Homology modeling and structure analysis

Multiple sequence alignments of putative PsXLNs with characterized XLNs were visualized using the Easy Sequencing in Postscript (<http://escript.ibcp.fr/EScript/EScript/>) [37]. Homology models were generated and evaluated according to the methods described elsewhere [38,39]. To obtain the enzyme-ligand complex and further explore how enzymes bind to WAX, models were superpositioned with known experimental 3D structures determined with ligands and visualized by PyMOL 2.3.5 (Schrödinger, Inc., New York, NY, USA) [39]. The models of GH10 XLNs were superpositioned with XA<sup>3</sup>X (subsite –1 to –3) from *Streptomyces olivaceoviridis* E-86 SoXyn10A (PDB ID: 1V6V) and X<sub>4</sub> (subsite +1 to +4) from *Caldicellulosiruptor bescii* CbXyn10C (PDB ID: 5OFK) [9,40]. The models of GH11 XLNs were superpositioned with XA<sup>3</sup>XX (subsite –1 to –4) from *S. olivaceoviridis* E-86 SoXyn11A (PDB ID: 7DFN) and X<sub>3</sub> (subsite +1 to +3) from *Trichoderma reesei* TrXyn11A

**Table 1**  
Biochemical properties of PsXLNs in this study.

GH family	Protein ID in JGI	Enzyme code	Optimum		Stability (>60%, 1 h)		Specific activity (U/μmol)	
			pH	Temperature	pH	Temperature	BWX	WAX
10	13043	PsXlnA	7	40	3–10	20–40	25301,5 ± 4069,6	15093,7 ± 562,8
	13445	PsXlnB <sup>a</sup>	7	70	3–11	20–50	9576,5 ± 613,5	5685,6 ± 386,3
	12441	PsXlnC	5	70	5–10	20–40	3326,5 ± 303,6	1997,1 ± 36,2
11	5870	PsXlnD	5	40	5–11	20–30	3242,7 ± 302,6	1744,5 ± 113,7
	9034	PsXlnE <sup>a</sup>	6	40	3–11	20–40	22280,5 ± 2263,1	12650,6 ± 1875,0
	1444	PsXlnF	6	70	6–8	20–30	2039,9 ± 136,0	1069,5 ± 210,8
	2115	PsXlnG	4	40	3–8	20–30	47,9 ± 11,6	16,6 ± 1,5
	3794	PsXlnH	6	40	3–11	20–30	5632,2 ± 384,5	3006,4 ± 195,9
	3721	PsXlnI <sup>a</sup>	4	70	3–8	20–30	175,6 ± 19,6	513,7 ± 12,6
	7375	PsXlnJ	5	40	3–8	20–40	0,3 ± 0,0	0,2 ± 0,0

<sup>a</sup> Enzyme possess a C-terminal CBM domain.

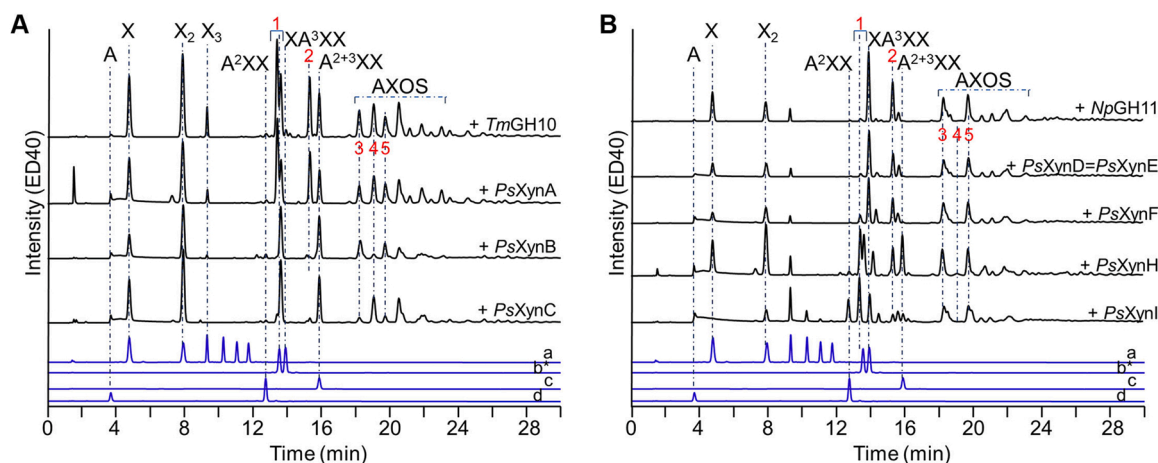


**Fig. 2.** HPAEC elution patterns of wheat arabinoxylan (WAX) digested with XLNs from GH10 (A) and GH11 (B) for 16 h. Arabinose (A), xylose (X), X<sub>2</sub>, X<sub>3</sub>, A<sup>2</sup>XX, XA<sup>2</sup>XX, XA<sup>3</sup>XX and A<sup>2+3</sup>XX were annotated based on analytical standards (bottom, a–d); other AXOS were annotated according to [36]; 1 = double peak due to co-elution of XA<sup>3</sup>X, XA<sup>2</sup>XX, A<sup>3</sup>X (elution order); 2 = XA<sup>2+3</sup>XX; 3 = XA<sup>3</sup>A<sup>3</sup>X; 4 = A<sup>3</sup>A<sup>3</sup>X; 5 = XA<sup>3</sup>A<sup>2+3</sup>XX; \*XA<sup>2</sup>XX eluted before XA<sup>3</sup>XX.

(PDB ID: 4HK8) [11,41].

## Results and discussion

### *P. subrubescens* harbors a high diversity of XLNs from GH10 and GH11

*P. subrubescens* stands out from most other *Penicillia*, as it contains an expanded set of genes encoding plant biomass-degrading enzymes, including genes encoding putative XLNs [14,19,42]. The JGI annotation for fungal genomes suggested that *P. subrubescens* contains three and seven members from GH10 and GH11, respectively, of which one of GH10 and two of GH11 contain a carbohydrate-binding module (CBM) domain in their sequence. To assess the diversity of these putative XLNs in *P. subrubescens* and their evolutionary relationship, PsXLNs from GH10 and GH11 were subjected to phylogenetic analysis with other fungal sequences from the corresponding family, including characterized enzymes (Fig. 1).

The three GH10 members in *P. subrubescens* showed clear evolutionary distances from each other in the phylogenetic tree, but each was located within a group of Eurotiomycete proteins, particularly from *Penicillia*, indicating that they are evolutionary conserved (Fig. 1A). PsXlnB with a C-terminal CBM domain clustered together with other Eurotiomycete sequences that contain a CBM domain, and showed very close relationship with *Talaromyces purpureogenus* XynD [43]. The close evolutionary distance between those enzymes may reflect similar properties. The presence of a CBM in XynD was speculated to be possibly involved in the binding of this enzyme to natural lignocellulosic substrates [43]. A similar consideration may be applied to the role of the

CBM in PsXlnB.

Similar to GH10, GH11 members in *P. subrubescens* clearly separated in the phylogenetic tree, indicating their phylogenetic diversity, with 3–4 members being present in each main branch of Eurotiomycete sequences (Fig. 1B). PsXlnG, PsXlnD, and PsXlnE were closer to each other than to any of the other enzymes. PsXlnE possesses a C-terminal CBM and clustered with other sequences from *Penicillium* species. Similarly, PsXlnF and PsXlnH were positioned more closely to each other than to other PsXLNs, and shared a same node with a small number of proteins from Dothideomycetes and Basidiomycetes in addition to those from Eurotiomycetes. The sequence feature of PsXlnI, similar to PsXlnE, harbored a CBM domain. But PsXlnI was located in a separate branch, which clustered very closely with a characterized *T. cellulolyticus* enzyme and with uncharacterized *Penicillium* proteins [44]. PsXlnJ was related to PsXlnF and PsXlnH, which split from the same node. Interestingly, the proteins clustered with PsXlnJ were mainly uncharacterized proteins from *Aspergillus* and other *Penicillium* species.

### PsXLNs have diverse biochemical properties

The cDNA fragments encoding XLNs in *P. subrubescens* were over-expressed in *P. pastoris*. Recombinant proteins were produced and purified (Supplementary Fig. S1). The functional characterization showed pH optima for PsXLNs ranged from acidic to neutral (pH 4–7), with most PsXLNs having temperature optima of 40 °C (Table 1). They are similar to the properties of characterized enzymes clustered with PsXLNs in the phylogenetic tree [45–50] (Fig. 1A). Surprisingly, four PsXLNs (PsXlnB and PsXlnC of GH10, and PsXlnI and PsXlnF of GH11) displayed the

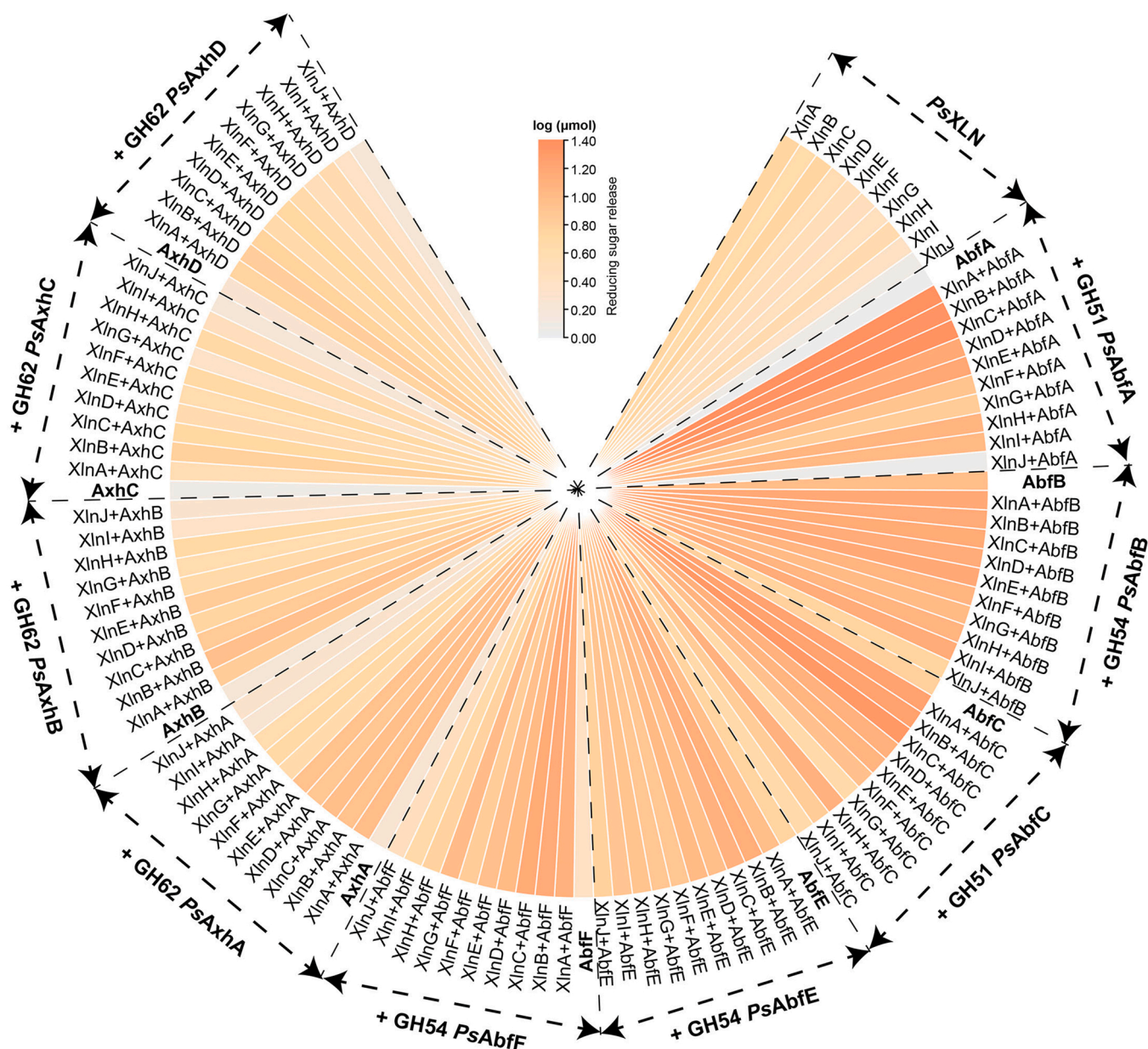


Fig. 3. Heatmap of reducing sugar released from 24 h incubation of wheat arabinoxylan by PsXLN with/without the addition of PsABF from GH51, GH54 and GH62. PsAbfA (JGI: 7770) and PsAbfC (JGI: 1664) belong to GH51; PsAbfB (JGI: 1940), PsAbfE (JGI: 3364), and PsAbfF (JGI: 6724) belong to GH54; PsAxA (JGI: 12472), PsAxB (JGI: 12883), PsAxC (JGI: 3399), and PsAxD (JGI: 6027) belong to GH62.

highest activity at 70 °C (Table 1).

All PsXLNs remained stable through the acidic to basic pH range, of which PsXlnB from GH10, and PsXlnH and PsXlnE from GH11 exhibited a significantly wider pH stability than others, as these enzymes retained > 60% of their residual activity after 1 h of incubation at pH 11.0 (Table 1). This high alkaline tolerance makes PsXLNs attractive for various higher pH biotechnological applications [51,52]. GH10 PsXLNs retained more than 60% residual activity after incubation at 40 °C for 1 h, while most GH11 PsXLNs retained similar activity after 1 h at 30 °C, with only PsXlnJ and PsXlnE being similar to GH10 XLNs (Table 1).

PsXLNs displayed higher specific activity on BWX than WAX, which is in line with commercially available XLNs [53] (Table 1). As an exception, PsXlnI from GH11 was more active on WAX than on BWX (Table 1). Additionally, among these different PsXLNs, PsXlnJ and PsXlnG showed the lowest specific activity against xylan substrates.

A previous study described the transcriptome response of *P. subrubescens* to arabinoxylan-rich wheat bran and pectin-rich sugar

beet pulp [42]. In this data set, the expression of the XLN-encoding genes from *P. subrubescens* grown on wheat bran was analyzed (Supplementary Table S3). The results revealed that all XLN-encoding genes were induced on wheat bran, with the highest induced expression being *xlnA* of GH10 and the lowest being *xlnJ* and *xlnG* in GH11. The low specific activity of PsXlnJ and PsXlnG against WAX may be related to the low expression of *xlnJ* and *xlnG* on wheat bran. However, it cannot be automatically concluded that the activity level of the enzymes and expression level of the corresponding genes correlate. PsXlnA and PsXlnE, as the most active enzymes towards WAX, showed similar activity levels, but the expression level of *xlnE* was about 4-fold higher than that of *xlnA*. Similar expression levels were observed in *xlnE* and *xlnF*, but the specific activity of PsXlnE towards WAX was 10-fold higher than that of PsXlnF. One possible reason for this could be that the media and culture conditions used do not reflect the heterogeneity and complexity of natural biotopes, and therefore may not reflect the natural response of *P. subrubescens*.

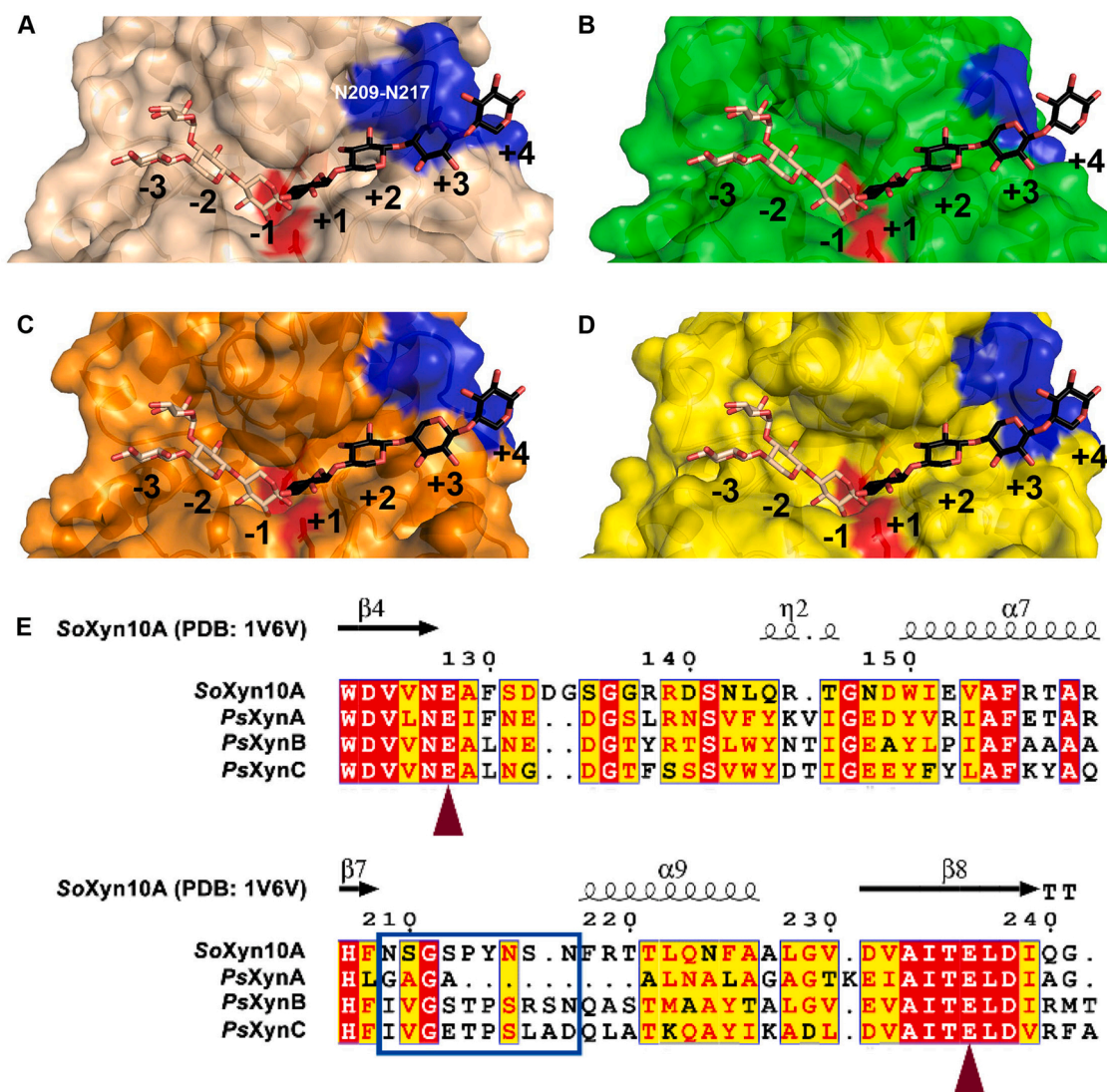


**Fig. 4.** Substrate-binding cleft of GH10 PsXLNs. (A) SoXyn10A (PDB: 1V6V); (B) PsXlnA, (C) PsXlnB; (D) PsXlnC. Crystal structure and homology models superimposed with  $XA^3X$  (subsite -1 to -3, shown as white sticks) and  $X_4$  (subsite +1 to +4, shown as black sticks); (E) Alignment of GH10 PsXLNs (PsXlnA-C) with *Streptomyces olivaceoviridis* SoXyn10A. Catalytic residues and the region of main difference ('N209-N217' region based on SoXyn10A) in the catalytic domain were highlighted using red triangles and blue box in (E), respectively, and in red and blue in (A)-(D).

#### PsXLNs have diverse product profiles

To obtain an insight into the mode of action of XLNs, the product profiles of each independent XLN incubated with WAX for 16 h (end-point incubations) were analyzed by HPSEC-RI and HPAEC-PAD. PsXlnJ and PsXlnG were excluded from the study of product profile due to their low activity against WAX. HPSEC-RI analysis showed the disappearance of soluble polymers (WAX around 300 kDa) and the shift of molecular weight distribution below 1 kDa after 16 h incubation (Supplementary Fig. S2), indicating that all tested PsXLNs could extensively degrade WAX. To complement HPSEC-RI, HPAEC-PAD analysis demonstrated the presence of both linear XOS and substituted AXOS as a consequence of WAX degradation by XLNs (Fig. 2).

$X_2$ ,  $XA^3A^3X$ ,  $XA^3A^{2+3}XX$ , and some unknown AXOS were clearly detected in all XLN-WAX digests, while the release of other annotated oligosaccharides (e.g.  $X_3$ ,  $XA^{2+3}XX$ ) was enzyme dependent (Fig. 2). A clear amount of xylose was also observed in XLN-WAX digests, except for the PsXlnI-WAX digest (Fig. 2B). The comparison of product profiles is discussed in detail below.

In addition to the common products observed in all XLN-WAX digests, all GH10 XLNs could release  $A^{2+3}XX$ ,  $A^3A^3X$ , and a trace amount

of  $A^2XX$  from WAX.  $XA^{2+3}XX$  was also detected in the PsXlnA- and TmGH10-WAX digests, which showed a more similar product profile to each other than to the others (Fig. 2A). The annotated 'peak 1' refers to a double peak due to the co-elution of  $XA^3X$ ,  $XA^2XX$ ,  $A^3X$ . The double peak of 'peak 1' was clearly observed in PsXlnA- and TmGH10-WAX digests, whereas PsXlnB- and PsXlnC-WAX digests showed only a single peak. This suggests that PsXlnA- and TmGH10-WAX digests contain more diverse components in 'peak 1'. Notably,  $X_3$  was present in PsXlnA-, PsXlnB- and TmGH10-WAX, expected to be an intermediate product, which is further hydrolyzed to  $X_2$  and xylose upon depletion of longer substrates.

Unlike GH10-WAX digests,  $X_3$  and  $XA^{2+3}XX$  were observed in all tested GH11-WAX digests.  $XA^3XX$  was also found in GH11-WAX except in the PsXlnH-WAX digest (Fig. 2B). Notably, some products were only present in specific XLN-WAX digests, such as  $A^2XX$  and  $A^{2+3}XX$  in PsXlnH- and PsXlnI-WAX digests, and longer XOS (degree of polymerization, DP >3) in the PsXlnI-WAX digest. In addition, PsXlnH- and PsXlnI-WAX digests contain a larger amount of product in 'peak 1'. Surprisingly, albeit only in trace amounts,  $A^3A^3X$  was present in the PsXlnH-WAX digest. In general, the product profiles of the PsXlnE-, PsXlnD- and PsXlnF-digests were similar to NpGH11 [35], while those of

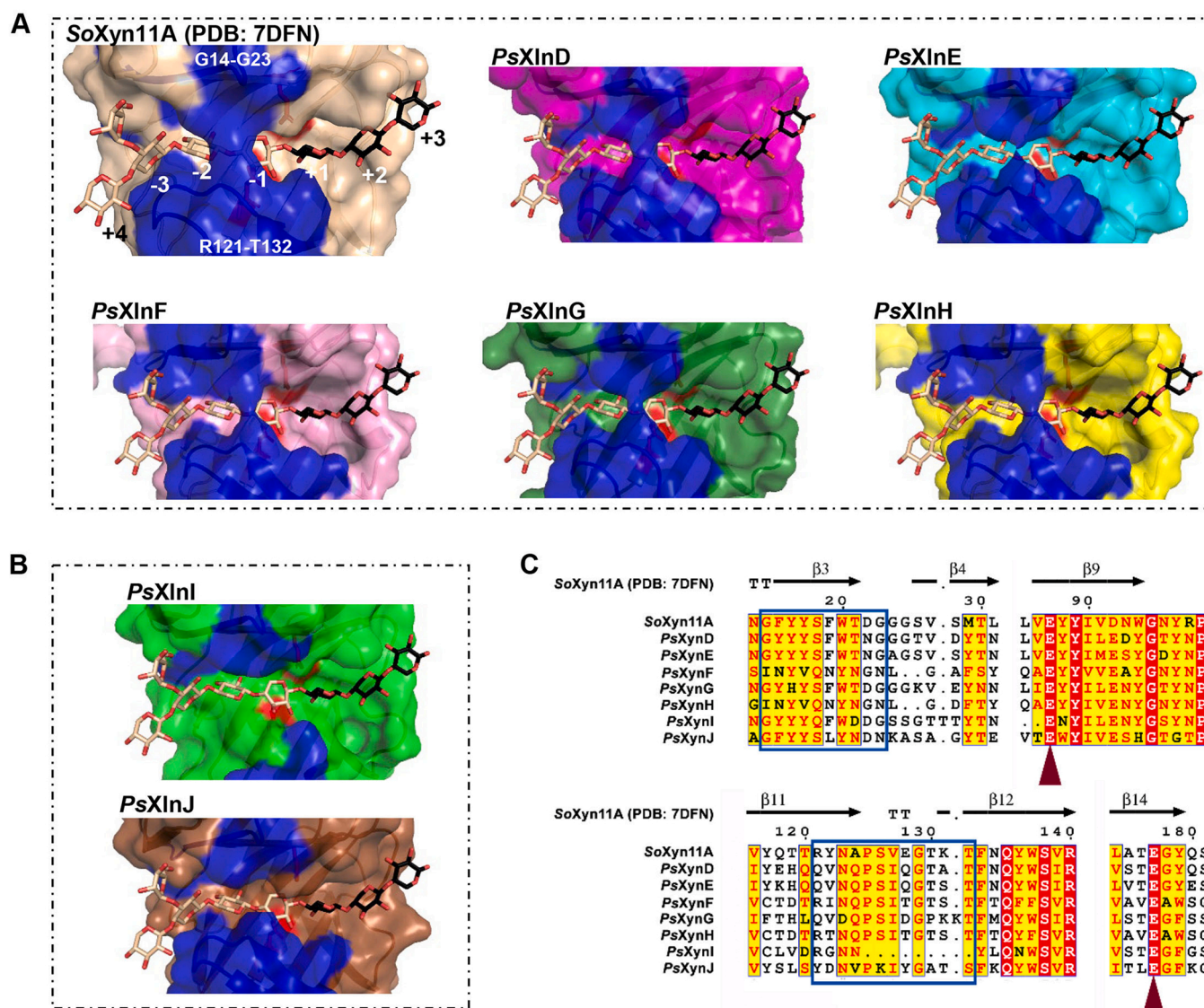


**Fig. 5.** Substrate-binding cleft of GH11 PsXLNs. (A) Crystal structure and homology models with a partially closed pocket; (B) Homology models with an open pocket. Crystal structure and homology models superpositioned with XA<sup>3</sup>XX (subsite -1 to -4, shown white sticks) and X<sub>3</sub> (subsite +1 to +3, shown black sticks); (C) Alignment of GH11 PsXLNs (PsXlnD-J) with *Streptomyces olivaceoviridis* SoXyn11A. Catalytic residues and “finger-thumb” (“G14-G23” and “R121-T132” regions based on SoXyn11A) in the catalytic domain were pointed out using red triangle and blue box in (C), respectively, and highlighted in red and blue in (A)-(B).

the PsXlnI- and PsXlnH-digests were more diverse.

The presence of XOS with mono-arabinosyl substitution at the O-2 position (e.g. A<sup>2</sup>XX, XA<sup>2</sup>XX) in XLN-WAX digests was unexpected, as this substitution in WAX has been reported only associated together with O-3 substitutions to form doubly substituted xylosyl residual [35,54]. The reason for the appearance of such products remains unclear. Further validation of the composition of the WAX used is needed.

*The addition of PsABFs to PsXLNs-WAX reaction enhanced reducing sugar release.*

A previous study confirmed that multiple GH51, GH54 and GH62 ABFs from *P. subrubescens* have the ability to degrade WAX and release arabinose, to varying degrees [21]. To effectively degrade WAX present in dietary fiber, the cooperative effect of PsXLNs with different PsABFs was evaluated here.

The addition of PsABFs improved the hydrolysis of WAX by PsXLNs to some extent, as indicated by the higher reducing sugar levels released from WAX by the combination of enzymes than by a single enzyme, especially in pairs of GH51 or GH54 PsABFs with PsXLNs (Fig. 3, Supplementary Table S4). Previous studies found that the simultaneous

addition of XLNs with GH51 or GH54 ABFs enhanced polysaccharide hydrolysis, achieving the highest sugar release compared to any enzyme alone or sequential addition of the enzymes [55–57]. Relative to GH51 or GH54 PsABFs, the overall cooperation of GH62 PsABFs with PsXLNs was weaker and some of the combinations, e.g. XlnA+AxhC, XlnC+AxhC, XlnI+AxhA, XlnA+AxhD, XlnI+AxhD, showed no or even a negative contribution in the reducing sugar release (Fig. 3, Supplementary Table S4). This could be explained by the high preference of GH62 PsABFs towards WAX rather than AXOS [58]. The cooperation effect for GH62 PsABFs and PsXLNs may be improved by sequential addition of the enzymes.

*Differences in the catalytic center of PsXLNs affect their hydrolysis behavior*

The differences observed in the product profiles of different PsXLNs in hydrolysis of WAX may be due to differences in their catalytic domain. Superposition models of PsXLNs on available crystal structures complexed with XOS/AXOS indicates interesting features in the

catalytic domain of models, which help to understand how the substrate binding cleft of PsXLNs is able to interact with WAX.

The superposition of structures of GH10 models and SoXyn10A (PDB: 1V6V) revealed that all GH10 PsXLNs can accommodate an L-arabinosyl side chain linked to O-3/O-2 at subsite – 3 and + 1, and O-3 at subsite – 2, which support certain products (e.g., A<sup>2+3</sup>XX, A<sup>3</sup>A<sup>3</sup>X, A<sup>2</sup>XX) released from the non-reducing end of WAX by GH10 PsXLNs [9,10] (Fig. 4A–D). Additionally, the loop in the “N209–N217” region (based on SoXyn10A) is far from the catalytic center of the models, which allows for more space in the catalytic domain, indicating that longer XOS (e.g. X<sub>3</sub>, X<sub>4</sub>) can be tolerated at the (+) subsite in catalytic cleft of GH10 PsXLNs [9] (Fig. 4B–D). A previous study has reported that some XLNs lacking a + 3 subsite can tolerate L-arabinosyl substituents at subsite + 2, whereas XLNs with a + 3 subsite cannot [10]. This inference may apply to GH10 models other than PsXlnA, which displays a wider cleft at subsite + 2 due to a shorter loop in “N209–N217” region (Fig. 4B, E; Supplementary Fig. S3). This structural feature might allow PsXlnA to accommodate substituted xylosyl at subsite + 2 (Fig. 4B), which could be an explanation for the presence of XA<sup>2+3</sup>XX in the PsXlnA–WAX digest (Fig. 2A). Moreover, the high tolerance of the active site of PsXlnA to L-arabinosyl decorations leads to the production of more diverse AXOS than the other GH10 PsXLNs upon WAX hydrolysis (Figs. 2A, 4B).

The comparison of structures between GH11 models and SoXyn11A (PDB: 7DFN) highlighted significant differences in the architecture of the catalytic center (termed “finger-thumb” regions) among the models, which is related to the different amino acids in the “G14–G23” and “R121–T132” regions and their arrangements in the catalytic domain [11] (Fig. 5, Supplementary Fig. S4). These differences were expected to be a major factor to explain their diverse product profiles (Fig. 2B). Generally, a partially closed conformation of “finger-thumb” regions is characteristic of the crystal structures of GH11 XLNs [59]. However, the corresponding region in several GH11 XLNs, i.e. PsXlnI and PsXlnJ, displays a fully open conformation, which makes the catalytic pocket more accessible (Fig. 5B). This may contribute to direct interactions with the substrate and the unique degradation pattern of WAX by these enzymes.

## Conclusions

Overall, the expansion of XLNs in the *P. subrubescens* genome was accompanied by functional diversity. Moreover, each independent XLN exhibited cooperative effects with *P. subrubescens* ABFs. These findings may reflect an evolutionary adaptation of this species that provides a wider enzymatic toolbox for synergistic degradation of hemicellulose in its natural habitat. Notably, the diverse product patterns of WAX hydrolysis by *P. subrubescens* XLNs results from the different features in their catalytic domain. This finding contributes to the understanding of the interaction between enzyme and decorated xylan, and provides leads for enzyme engineering towards tailor-made XLNs.

## CRedit authorship contribution statement

RPdV conceived and supervised the overall project. RPdV and MAK designed the experiment. XL and DK conducted the experiments. XL wrote the original draft. All authors analyzed the data and commented on the manuscript.

## Declaration of Competing Interest

The authors declare that they have no known competing financial interests or personal relationships that could have appeared to influence the work reported in this paper.

## Acknowledgements

The authors thank MSc Astrid Mueller for assistance with HPLC, Dr.

Sumitha Krishnaswamyreddy for advice on structure analysis, and Dr. Adiphool Dilokpimol for suggestions on gene cloning. XL was supported by the China Scholarship Council for financial support (grant no. 201803250066).

## Appendix A. Supporting information

Supplementary data associated with this article can be found in the online version at doi:10.1016/j.nbt.2022.05.004.

## References

- [1] Hansen CM, Björkman A. The ultrastructure of wood from a solubility parameter point of view. *Holzforschung* 1998;52:335–44. <https://doi.org/10.1515/hfsg.1998.52.4.335>.
- [2] Terrett OM, Lyczakowski JJ, Yu L, Iuga D, Franks WT, Brown Steven P, et al. Molecular architecture of softwood revealed by solid-state NMR. *Nat Commun* 2019;10:1–11. <https://doi.org/10.1038/s41467-019-12979-9>.
- [3] Amorim C, Silvério SC, Prather KLJ, Rodrigues LR. From lignocellulosic residues to market: production and commercial potential of xylooligosaccharides. *Biotechnol Adv* 2019;37:107397. <https://doi.org/10.1016/j.biotechadv.2019.05.003>.
- [4] Lombard V, Golaconda RH, Drula E, Coutinho PM, Henrissat B. The carbohydrate-active enzymes database (CAZY) in 2013. *Nucleic Acids Res* 2014;42:D490–5. <https://doi.org/10.1093/nar/gkt1178>.
- [5] Bastawde KB. Xylan structure, microbial xylanases, and their mode of action. *World J Microbiol Biotechnol* 1992;8:353–68. <https://doi.org/10.1007/BF01198746>.
- [6] Paës G, Berrin JG, Beaugrand J. GH11 xylanases: structure/function/properties relationships and applications. *Biotechnol Adv* 2012;30:564–92. <https://doi.org/10.1016/j.biotechadv.2011.10.003>.
- [7] Pollet A, Delcour JA, Courtin CM. Structural determinants of the substrate specificities of xylanases from different glycoside hydrolase families. *Crit Rev Biotechnol* 2010;30:176–91. <https://doi.org/10.3109/07388551003645599>.
- [8] Capetti CCM, Vacilotto MM, Dabul ANG, Sepulchro AGV, Pellegrini VOA, Polikarpov I. Recent advances in the enzymatic production and applications of xylooligosaccharides. *World J Micro Biotechnol* 2021;37:1–12. <https://doi.org/10.1007/s11274-021-03139-7>.
- [9] Fujimoto Z, Kaneko S, Kuno A, Kobayashi H, Kusakabe I, Mizuno H. Crystal structures of decorated xylooligosaccharides bound to a family 10 xylanase from *Streptomyces olivaceoviridis* E-86. *J Biol Chem* 2004;279:9606–14. <https://doi.org/10.1074/jbc.M312293200>.
- [10] Pell G, Taylor EJ, Gloster TM, Turkenburg JP, Fontes CMGA, Ferreira LMA, et al. The mechanisms by which family 10 glycoside hydrolases bind decorated substrates. *J Biol Chem* 2004;279:9597–605. <https://doi.org/10.1074/jbc.M312278200>.
- [11] Fujimoto Z, Kishine N, Teramoto K, Tsutsui S, Kaneko S. Structure-based substrate specificity analysis of GH11 xylanase from *Streptomyces olivaceoviridis* E-86. *Appl Microbiol Biotechnol* 2021;105:1943–52. <https://doi.org/10.1007/s00253-021-11098-0>.
- [12] Hu J, Saddler JN. Why does GH10 xylanase have better performance than GH11 xylanase for the deconstruction of pretreated biomass? *Biomass Bioenergy* 2018; 110:13–6. <https://doi.org/10.1016/j.biombioe.2018.01.007>.
- [13] Polizeli MLTM, Rizzatti ACS, Monti R, Terenzi HF, Jorge JA, Amorim DS. Xylanases from fungi: properties and industrial applications. *Appl Microbiol Biotechnol* 2005; 67:577–91. <https://doi.org/10.1007/s00253-005-1904-7>.
- [14] Li X, Dilokpimol A, Kabel MA, de Vries RP. Fungal xylanolytic enzymes: diversity and applications. *Bioresour Technol* 2022;344:126290. <https://doi.org/10.1016/j.biortech.2021.126290>.
- [15] Dar FM, Dar Parsa M. Fungal xylanases for different industrial applications. In: Ahmed MAA, Ajar NY, Neelam Y, Minaxi S, editors. *Industrially important fungi for sustainable development*. Cham: Springer; 2021. p. 515–39. [https://doi.org/10.1007/978-3-030-85603-8\\_14](https://doi.org/10.1007/978-3-030-85603-8_14).
- [16] Bhardwaj N, Agrawal K, Verma P. Xylanases: an overview of its diverse function in the field of biorefinery. In: Manish S, Neha S, Rajeev S, editors. *Bioenergy research: commercial opportunities & challenges*. Singapore: Springer; 2021. p. 295–317. [https://doi.org/10.1007/978-981-16-1190-2\\_10](https://doi.org/10.1007/978-981-16-1190-2_10).
- [17] Aguilar-Pontes MV, Brandl J, McDonnell E, Strasser K, Nguyen TTM, Riley R, et al. The gold-standard genome of *Aspergillus niger* NRRL 3 enables a detailed view of the diversity of sugar catabolism in fungi. *Stud Mycol* 2018;91:61–78. <https://doi.org/10.1016/j.simyco.2018.10.001>.
- [18] Martinez D, Berka RM, Henrissat B, Saloheimo M, Arvas M, Baker SE, et al. Genome sequencing and analysis of the biomass-degrading fungus *Trichoderma reesei* (syn. *Hypocrea jecorina*). *Nat Biotechnol* 2008;26:553–60. <https://doi.org/10.1038/nbt1403>.
- [19] Peng M, Dilokpimol A, Mäkelä MR, Hildén K, Bervoets S, Riley R, et al. The draft genome sequence of the ascomycete fungus *Penicillium subrubescens* reveals a highly enriched content of plant biomass related CAZymes compared to related fungi. *J Biotechnol* 2017;246:1–3. <https://doi.org/10.1016/j.jbiotec.2017.02.012>.
- [20] Linares NC, Dilokpimol A, Ståhlbrand H, Mäkelä MR, de Vries RP. Recombinant production and characterization of six novel GH27 and GH36  $\alpha$ -galactosidases from *Penicillium subrubescens* and their synergism with a commercial mannanase

- during the hydrolysis of lignocellulosic biomass. *Bioresour Technol* 2020;295:122258. <https://doi.org/10.1016/j.biortech.2019.122258>.
- [21] Coconi LN, Li X, Dilokpimol A, de Vries RP. Comparative characterization of nine novel GH51, GH54 and GH62  $\alpha$ -L-arabinofuranosidases from *Penicillium subrubescens*. *FEBS Lett* 2022;596:360–8. <https://doi.org/10.1002/1873-3468.14278>.
- [22] Grigoriev IV, Nikitin R, Haridas S, Kuo A, Ohm R, Otilar R, et al. MycoCosm portal: gearing up for 1000 fungal genomes. *Nucleic Acids Res* 2014;42:D699–704. <https://doi.org/10.1093/nar/gkt1183>.
- [23] Armenteros JJA, Tsirigos KD, Sønderby CK, Petersen TN, Winther O, Brunak S, et al. SignalP 5.0 improves signal peptide predictions using deep neural networks. *Nat Biotechnol* 2019;37:420–3. <https://doi.org/10.1038/s41587-019-0036-z>.
- [24] Katoh K, Rozewicki J, Yamada KD. MAFFT online service: multiple sequence alignment, interactive sequence choice and visualization. *Brief Bioinform* 2019;20:1160–6. <https://doi.org/10.1093/bib/bbx108>.
- [25] Kumar S, Stecher G, Tamura K. MEGA7: molecular evolutionary genetics analysis version 7.0 for bigger datasets. *Mol Biol Evol* 2016;33:1870–4. <https://doi.org/10.1093/molbev/msw054>.
- [26] Van CS, Volckaert G. Differential expression of endo-beta-1,4-xylanase isoenzymes X-I and X-II at various stages throughout barley development. *Plant Sci* 2005;169:512–22. <https://doi.org/10.1016/j.plantsci.2005.05.003>.
- [27] Chen NJ, Paul RE. Endoxylanase expressed during papaya fruit ripening purification cloning and characterization. *Funct Plant Biol* 2003;30:433–41. <https://doi.org/10.1071/FP02208>.
- [28] Bih FY, Wu SS, Ratnayake C, Walling LL, Nothnagel EA, Huang AH. The predominant protein on the surface of maize pollen is an endoxylanase synthesized by a tapetum mRNA with a long 5' leader. *J Biol Chem* 1999;274:22884–94. <https://doi.org/10.1074/jbc.274.32.22884>.
- [29] Kunst F, Ogasawara N, Moszer I, Albertini AM, Alloni G, Azevedo V, et al. The complete genome sequence of the gram-positive bacterium *Bacillus subtilis*. *Nature* 1997;390:249–56. <https://doi.org/10.1038/36786>.
- [30] Millward-Sadler SJ, Poole D, Henrissat B, Hazlewood G, Clarke JH, Gilbert HJ. Evidence for a general role for high-affinity non-catalytic domains in microbial plant cell wall hydrolases. *Mol Microbiol* 1994;11:375–82. <https://doi.org/10.1111/j.1365-2958.1994.tb00317.x>.
- [31] DeBoy RT, Mongodin EF, Fouts DE, Tailford LE, Khouri H, Emerson JB, et al. Insights into plant cell wall degradation from the genome sequence of the soil bacterium *Cellvibrio japonicus*. *J Bacteriol* 2008;190:5455–63. <https://doi.org/10.1128/JB.01701-07>.
- [32] Li X, Griffin K, Langeveld S, Frommhagen M, Underlin EN, Kabel MA, et al. Functional validation of two fungal subfamilies in carbohydrate esterase family 1 by biochemical characterization of esterases from uncharacterized branches. *Front Bioeng Biotech* 2020;8:694. <https://doi.org/10.3389/fbioe.2020.00694>.
- [33] Lindsay H. A colorimetric estimation of reducing sugars in potatoes with 3, 5-dinitrosalicylic acid. *Potato Res* 1973;16:176–9. <https://doi.org/10.1007/BF02356048>.
- [34] Van Gool MP, Toth K, Schols HA, Szakacs G, Gruppen H. Performance of hemicellulolytic enzymes in culture supernatants from a wide range of fungi on insoluble wheat straw and corn fiber fractions. *Bioresour Technol* 2012;114:523–8. <https://doi.org/10.1016/j.biortech.2012.03.037>.
- [35] McCleary BV, McKie VA, Draga A, Rooney E, Mangan D, Larkin J. Hydrolysis of wheat flour arabinoxylan, acid-debranched wheat flour arabinoxylan and arabinoxylo-oligosaccharides by  $\beta$ -xylanase,  $\alpha$ -L-arabinofuranosidase and  $\beta$ -xylosidase. *Carbohydr Res* 2015;407:79–96. <https://doi.org/10.1016/j.carres.2015.01.017>.
- [36] Van Laere KMJ, Voragen CHL, Kroef T, Van den BLAM, Beldman G, Voragen AGJ. Purification and mode of action of two different arabinoxylan arabinofuranohydrolases from *Bifidobacterium adolescentis* DSM 20083. *Appl Microbiol Biotechnol* 1999;51:606–13. <https://doi.org/10.1007/s002530051439>.
- [37] Gouet P, Courcelle E, Stuart DI, Metz F. ESPript: analysis of multiple sequence alignments in PostScript. *Bioinformatics* 1999;15:305–8. <https://doi.org/10.1093/bioinformatics/15.4.305>.
- [38] Li X, Kouzounis D, Kabel MA, de Vries RP, Dilokpimol A. Glycoside Hydrolase family 30 harbors fungal subfamilies with distinct polysaccharide specificities. *N Biotechnol* 2022;67:32–41. <https://doi.org/10.1016/j.nbt.2021.12.004>.
- [39] DeLano WL. Pymol: an open-source molecular graphics tool. *CCP4 Newsl Protein Crystallogr* 2002;40:82–92.
- [40] Chu Y, Tu T, Penttinen L, Xue X, Wang X, Yi Z, et al. Insights into the roles of non-catalytic residues in the active site of a GH10 xylanase with activity on cellulose. *J Biol Chem* 2017;292:19315–27. <https://doi.org/10.1074/jbc.M117.807768>.
- [41] Wan Q, Zhang Q, Hamilton-Brehm S, Weiss K, Mustyakimov M, Coates L, et al. X-ray crystallographic studies of family 11 xylanase Michaelis and product complexes: implications for the catalytic mechanism. *Acta Crystallogr D Biol Crystallogr* 2014;70:11–23. <https://doi.org/10.1107/S1399004713023626>.
- [42] Dilokpimol A, Peng M, Di Falco M, Woeng TCA, Hegi RMW, Granchi Z, et al. *Penicillium subrubescens* adapts its enzyme production to the composition of plant biomass. *Bioresour Technol* 2020;311:123477. <https://doi.org/10.1016/j.biortech.2020.123477>.
- [43] Echeverría V, Eyzaguirre J. *Penicillium purpurogenum* produces a set of endoxylanases: identification, heterologous expression, and characterization of a fourth xylanase, XynD, a novel enzyme belonging to glycoside hydrolase family 10. *Appl Biochem Biotechnol* 2019;187:298–309. <https://doi.org/10.1007/s12010-018-2782-7>.
- [44] Watanabe M, Inoue H, Inoue B, Yoshimi M, Fujii T, Ishikawa K. Xylanase (GH11) from *Acremonium cellulolyticum*: homologous expression and characterization. *AMB Exp* 2014;4:1–8. <https://doi.org/10.1186/s13568-014-0027-x>.
- [45] Laothanachareon T, Bunternngsook B, Suwannarangsee S, Eurwilachit L, Champreda V. Synergistic action of recombinant accessory hemicellulolytic and pectinolytic enzymes to *Trichoderma reesei* cellulase on rice straw degradation. *Biores Technol* 2015;198:682–90. <https://doi.org/10.1016/j.biortech.2015.09.053>.
- [46] Sydenham R, Zheng Y, Riemens A, Tsang A, Powlowski J, Storms R. Cloning and enzymatic characterization of four thermostable fungal endo-1,4- $\beta$ -xylanases. *Appl Microbiol Biotechnol* 2014;98:3613–28. <https://doi.org/10.1007/s00253-013-5244-8>.
- [47] Takahashi Y, Kawabata H, Murakami S. Analysis of functional xylanases in xylan degradation by *Aspergillus niger* E-1 and characterization of the GH family 10 xylanase XynVII. *Springerplus* 2013;2:1–11. <https://doi.org/10.1186/2193-1801-2-447>.
- [48] Wang J, Mai G, Liu G, Yu S. Molecular cloning and heterologous expression of an acid-stable endoxylanase gene from *Penicillium oxalicum* in *Trichoderma reesei*. *J Microbiol Biotechnol* 2013;23:251–9.
- [49] Xiong K, Hou J, Jiang Y, Li X, Teng C, Li Q, et al. Mutagenesis of N-terminal residues confer thermostability on a *Penicillium janthinellum* MA21601 xylanase. *BMC Biotechnol* 2019;19:1–9. <https://doi.org/10.1186/s12896-019-0541-7>.
- [50] Yang Y, Yang J, Wang R, Liu J, Zhang Y, Liu L, et al. Cooperation of hydrolysis modes among xylanases reveals the mechanism of hemicellulose hydrolysis by *Penicillium chrysogenum* P33. *Micro Cell Fact* 2019;18:1–13. <https://doi.org/10.1186/s12934-019-1212-z>.
- [51] Anthony T, Raj KC, Rajendran A, Gunasekaran P. High molecular weight cellulase-free xylanase from alkali-tolerant *Aspergillus fumigatus* ARI. *Enzym Micro Technol* 2003;32:647–54. [https://doi.org/10.1016/S0141-0229\(03\)00050-4](https://doi.org/10.1016/S0141-0229(03)00050-4).
- [52] Taneja K, Gupta S, Kuhad RC. Properties and application of a partially purified alkaline xylanase from an alkalophilic fungus *Aspergillus nidulans* KK-99. *Bioresour Technol* 2002;85:39–42. [https://doi.org/10.1016/S0960-8524\(02\)00064-0](https://doi.org/10.1016/S0960-8524(02)00064-0).
- [53] Mangan D, Cornaggia C, Liadova A, McCormack N, Ivory R, McKie VA, et al. Novel substrates for the automated and manual assay of endo-1,4- $\beta$ -xylanase. *Carbohydr Res* 2017;445:14–22. <https://doi.org/10.1016/j.carres.2017.02.009>.
- [54] Sørensen HR, Pedersen S, Jørgensen CT, Meyer AS. Enzymatic hydrolysis of wheat arabinoxylan by a recombinant “minimal” enzyme cocktail containing  $\beta$ -xylosidase and novel endo-1,4- $\beta$ -xylanase and  $\alpha$ -L-arabinofuranosidase activities. *Biotechnol Prog* 2007;23:1000–7. <https://doi.org/10.1021/bp0601701>.
- [55] De Wet BJM, Matthew MKA, Storbeck KaH, Van Zyl WH, Prior BA. Characterization of a family 54  $\alpha$ -L-arabinofuranosidase from *Aureobasidium pullulans*. *Appl Microbiol Biotechnol* 2008;77:975–83. <https://doi.org/10.1007/s00253-007-1235-y>.
- [56] Tu T, Li X, Meng K, Bai Y, Wang Y, Wang Z, et al. A GH51  $\alpha$ -L-arabinofuranosidase from *Talaromyces leycettanus* strain JCM12802 that selectively drives synergistic lignocellulose hydrolysis. *Micro Cell Fact* 2019;18:1–12. <https://doi.org/10.1186/s12934-019-1192-z>.
- [57] Yang W, Bai Y, Yang P, Luo H, Huang H, Meng K, et al. A novel bifunctional GH51 exo- $\alpha$ -L-arabinofuranosidase/endo-xylanase from *Alicyclobacillus* sp. A4 with significant biomass-degrading capacity. *Biotechnol Biofuels* 2015;8:1–11. <https://doi.org/10.1186/s13068-015-0366-0>.
- [58] Wilkens C, Andersen S, Dumon C, Berrin JG, Svensson B. GH62 arabinofuranosidases: structure, function and applications. *Biotechnol Adv* 2017;35:792–804. <https://doi.org/10.1016/j.biotechadv.2017.06.005>.
- [59] Törrönen A, Harkki A, Rouvinen J. Three-dimensional structure of endo-1,4-beta-xylanase II from *Trichoderma reesei*: two conformational states in the active site. *EMBO J* 1994;13:2493–501. <https://doi.org/10.1002/j.1460-2075.1994.tb06536.x>.